

Oxygen Isotope Exchange between Carbon Dioxide and Iron Oxides on Mars' Surface

Sándor Góbi, Zhou Lin, Cheng Zhu, Martin Head-Gordon,* and Ralf I. Kaiser*

Cite This: *J. Phys. Chem. Lett.* 2022, 13, 2600–2606

Read Online

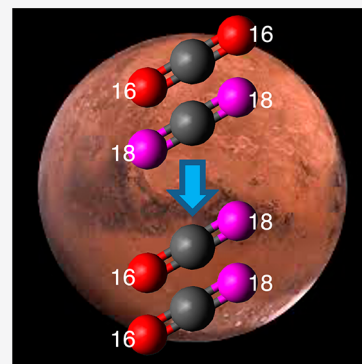
ACCESS |

Metrics & More

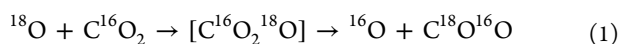
Article Recommendations

Supporting Information

ABSTRACT: An investigation of the fundamental processes leading to the incorporation of ^{18}O isotopes in carbon dioxide and in iron oxides is critical to understanding the atmospheric evolution and geochemistry of Mars. Whereas signatures of ^{18}O have been observed by the Phoenix Lander and the sample analysis at Mars for carbon dioxide, the underlying isotopic exchange pathways with minerals of the crust of Mars are still elusive. Here, we reveal that reactions of gaseous ^{18}O -carbon dioxide over goethite ($\text{FeO}(\text{OH})$) and hematite (Fe_2O_3) lead to an ^{18}O transfer from the atmosphere that enriches the ^{18}O content of the iron oxides in the absence of water and light. This proof-of-concept study shows that isotopic enrichment processes on Mars not only are limited to the atmosphere but also proceed via chemical interaction with dry iron oxides. These processes are decisive to comprehending the ^{18}O cycle between the atmosphere and the surface on the planetary scale.



Bimolecular gas-phase reactions of electronically excited atomic oxygen ($^{18}\text{O}(^1\text{D})$) with carbon dioxide involving carbon trioxide (CO_3) intermediates have been hypothesized to drive the ^{18}O isotopic enrichment in carbon dioxide in the Martian atmosphere (reaction 1),^{1–3} whereas an examination of the isotopic composition data of Martian meteorites hints at mineral-mediated isotopic enrichment processes.^{4,5}



Heterogeneous isotopic exchanges between atmospheric ^{18}O -carbon dioxide and oxygen-bearing minerals such as iron oxides have been proposed as sources of isotopic fractionation, but these processes operate only at temperatures beyond 800 K,⁶ vastly exceeding even the highest temperature on Mars recorded at the equator of 300 K by Viking Landers, Mars Global Surveyor, Mars Exploration Rovers, Odyssey Orbiter, and Mars Reconnaissance Orbiter.^{7–11} However, it is also known that CO_2 exchanges O with surfaces of hydrated salts at lab temperatures or even with dry glass.¹² An ultraviolet photon-assisted oxygen isotope fractionation in the presence of liquid water has been demonstrated to lead to $\delta^{18}\text{O} = +6\text{‰}$ compared to the VSMOW (Vienna Standard Mean Ocean Water) value, but this mechanism applies only if shallow standing water on Mars could persist over geological time scales in the past.^{13,14} Despite the relatively low concentration of only 1%, carbonates are the most intriguing constituents of Mars-related meteorites, as they were likely formed from the interaction of atmospheric carbon dioxide and water.^{15–19} On the basis of an isotopic analysis of the ALH84001 meteorite and laboratory studies, Thiemens et al. proposed a transfer of oxygen isotopes from atmospheric ozone to carbonates via

hydrogen peroxide when ozone reacts with surface-bound water on atmospheric aerosols.²⁰ This mechanism may provide an explanation for the production of isotopically anomalous carbonates found in the SNC (shergottites, nakhlites, chassignites) Martian meteorites.^{19,21} Consequently, laboratory and modeling investigations on oxygen isotope exchange in the Martian atmosphere and on the surface have been expanded to elucidate potential heterogeneous surface processes involving gas–liquid exchanges between carbon dioxide (CO_2) and water (H_2O).^{22–24} Isotopic exchange reactions between gaseous carbon dioxide with metal oxides such as zinc oxide have also been performed, although the experimental parameters do not replicate the surface conditions on Mars (Supporting Information, Table S1).

Thus, despite more than half a century of research, the fundamental ^{18}O isotopic exchange pathways between atmospheric molecules with minerals prevailing on the surface of Mars are still elusive, although they are critical to rationalize the full oxygen cycle between the atmosphere and the Martian surface on the planetary scale. Here, we reveal a significant, hitherto overlooked ^{18}O isotopic exchange process between carbon dioxide as the predominant constituent of the atmosphere on Mars (94.9%) with prevalent iron oxides existing as hematite (Fe_2O_3) and goethite ($\text{FeO}(\text{OH})$). Up to

Received: January 29, 2022

Accepted: March 3, 2022

Published: March 15, 2022



49% of iron may be incorporated in hematite and up to 40% in goethite as determined by the Spirit Rover in the Gusev Crater; these minerals are supplemented by, for example, pyroxene, olivine, and jarosite.²⁵ These minerals are hence widely used by the planetary science community as constituents of Mars analog soils.^{26–28} Our studies reveal that reactions of gaseous ¹⁸O-carbon dioxide over goethite and hematite lead to a substantial ¹⁸O transfer from the gas phase to the iron oxides at the temperature of 293 K even in the absence of water. Complementary electronic structure calculations are in accord with our experimental findings and suggest preferential incorporation of ¹⁸O in goethite (FeO(OH)) compared to hematite (Fe₂O₃). Thus, this proof-of-concept study shows that isotopic enrichment processes on Mars are more complex than previously thought and implicates heterogeneous chemistry involving distinct iron oxides without a requirement for surface water. Our results bring us closer to an understanding of the isotope exchange processes via heterogeneous chemistry taking place on Mars and the resulting ¹⁸O enrichment in Martian meteorites.

Figure 1 visualizes the temporal evolution of the normalized ion counts of three isotopologues of carbon dioxide recorded

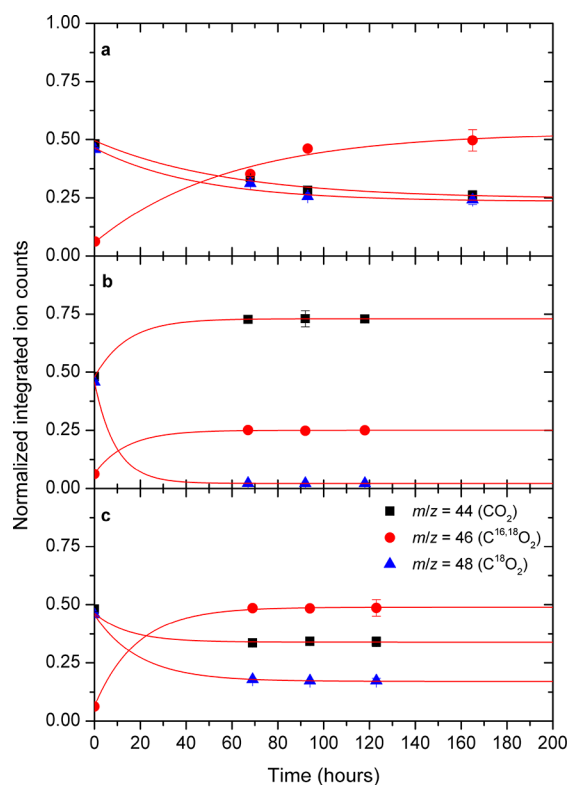


Figure 1. Normalized and integrated EI-QMS temporal profiles of the C¹⁶O₂–C¹⁸O₂ system. The data are shown for *m/z* values of 44 (C¹⁶O₂, black squares), 46 (C¹⁶O¹⁸O₂, red circles), and 48 (C¹⁸O₂, blue triangles) from a Pyrex vial that (a) does not contain any iron oxides, (b) contains FeO(OH), and (c) contains Fe₂O₃, respectively. The error bars of the data points represent the calculated standard deviation of 10 EI-QMS cycles, each accumulated for 25 s.

at mass-to-charge (*m/z*) ratios of 44 (C¹⁶O₂), 46 (C¹⁶O¹⁸O), and 48 (C¹⁸O₂) obtained while effusing each of the gas mixtures at distinct time intervals into the ultrahigh-vacuum chamber. The time zero defines the fraction of the initial ion counts for *m/z* = 44 (C¹⁶O₂), 46 (C¹⁶O¹⁸O), and 48 (C¹⁸O₂)

to be 48 ± 1%, 6 ± 1%, and 46 ± 1%, respectively. It should be noted that under ideal conditions only ion counts of *m/z* = 44 (C¹⁶O₂) and 48 (C¹⁸O₂) should be present; the detection of *m/z* = 46 (C¹⁶O¹⁸O) reflects deviations from purity of the C¹⁸O₂ sample. In the reference sample (Figure 1a), both C¹⁶O₂ and C¹⁸O₂ decrease over time from 48 ± 1% and 46 ± 1% to 26 ± 1% and 24 ± 1%, respectively. Simultaneously, the fraction of C¹⁶O¹⁸O increases from 6 ± 1% to 50 ± 1%. The overall fraction of the ¹⁶O and ¹⁸O isotopes remains constant within the error limits at 51 ± 2% and 49 ± 2%, respectively. The enhancement of C¹⁸O¹⁶O suggests that an isotopic exchange must exist at 293 K between C¹⁸O₂ and C¹⁶O₂, as expected from a statistical isotopic exchange. While oxygen exchange between carbon dioxide isotopologues in the gas phase has not been studied experimentally or theoretically to our knowledge, a bimolecular gas-phase reaction 2 between both isotopologue reactants C¹⁸O₂ and C¹⁶O₂ (both being stable closed shell molecules) should face a significant activation barrier, which cannot be overcome at 293 K. Therefore, it cannot account for the oxygen isotopic exchange as detected experimentally. On the other hand, the surface of the Pyrex glass, a boron–silicate glass which consists of 80.6% SiO₂, 12.6% B₂O₃, 4.2% Na₂O, 2.2% Al₂O₃, 0.1% CaO, 0.1% Cl, 0.05% MgO, and 0.04% Fe₂O₃, may catalyze the isotopic exchange between C¹⁸O₂ and C¹⁶O₂ (Table S1). However, the constant fraction of ¹⁶O and ¹⁸O of 51 ± 2% and 49 ± 2% before and after the reaction reveals that no ¹⁶O from the Pyrex glass has been exchanged with ¹⁸O from carbon dioxide (C¹⁸O₂). Therefore, we can conclude that the presence of the reaction vessel does not lead to a depletion of ¹⁸O from the gas phase but does catalyze oxygen exchange between C¹⁸O₂ and C¹⁶O₂.



In strong and intriguing contrast to the aforementioned findings in the reference sample, carbon dioxide over Fe₂O₃ and in particular over FeO(OH) gets depleted in ¹⁸O at the end of the reaction. Quantitatively, the final fractions of C¹⁶O₂ to C¹⁸O₂ to C¹⁶O¹⁸O of 34 ± 1% to 17 ± 1% to 49 ± 2% (Fe₂O₃) and 73 ± 1% to 2 ± 1% to 25 ± 1% (FeO(OH)) translate into overall ¹⁶O to ¹⁸O fractions of 60 ± 2% to 40 ± 2% (Fe₂O₃) and 86 ± 2% to 14 ± 2% (FeO(OH)) at the end of the experiments compared to 51 ± 2% to 49 ± 2% when the reaction started. The gas-phase depletion of ¹⁸O suggests an efficient exchange with ¹⁶O from the condensed phase (i.e., Fe₂O₃ and FeO(OH)) and hence an enrichment of ¹⁸O in the iron oxides even at 293 K. This enrichment is significantly more pronounced in the FeO(OH) sample, thus underlining the conceptual framework of an enhanced catalytic activity of FeO(OH) compared to Fe₂O₃. Water adsorbed on the iron oxide surfaces could play a role in the isotope exchange; however, no traces of water could be detected in our samples (Figure S1 and Table S2).

The temporal profiles in Figure 1 are fitted and the rate constants are exploited to gain additional information about the isotopic enrichment processes. In detail, eqs 3 and 4 of a (pseudo) first-order process can be utilized to fit the decay and growth curves (Table 1), where *I_i(t)* equals the normalized ion counts at a given time *t* (s) and *k_i* is the rate constant (s⁻¹) of the *i*th species.²⁹

$$I_i(t) = I_i(0) \exp(k_i t) \quad (3)$$

Table 1. Decay–Growth Rate Constants (in s⁻¹) for the Experiments as Derived from the EI-QMS Temporal Profiles

type of experiment	species of interest (<i>m/z</i>)		
	C ¹⁶ O ₂ (44)	C ¹⁶ O ¹⁸ O (46)	C ¹⁸ O ₂ (48)
without iron oxides	(3.3 ± 0.9) × 10 ⁻⁶	(4.8 ± 2.0) × 10 ⁻⁶	(4.3 ± 1.3) × 10 ⁻⁶
FeO(OH)	(2.0 ± 0.1) × 10 ⁻⁵	(2.0 ± 0.1) × 10 ⁻⁵	(2.1 ± 0.1) × 10 ⁻⁵
Fe ₂ O ₃	(1.3 ± 0.1) × 10 ⁻⁵	(1.5 ± 0.1) × 10 ⁻⁵	(9.9 ± 0.1) × 10 ⁻⁶

$$I_i(t) = I_i(0)[1 - \exp(-k_i t)] + I_i(t = \infty) \quad (4)$$

According to the data, the rate constants associated with the formation (C¹⁶O¹⁸O) and decay (C¹⁶O₂, C¹⁸O₂) of the isotopologues in the reference sample are identical within the error limits. The rate constants in the Fe₂O₃-containing sample are 2–4 times higher than the decay and formation rates obtained from the reference sample. On the other hand, the rates in the FeO(OH) system increase by close to 1 order of magnitude. This underscores the more efficient ¹⁸O depletion from the gas phase into the condensed-phase FeO(OH) catalyst. These findings also underscore the earlier conclusion that FeO(OH) is more active for ¹⁸O incorporation than Fe₂O₃.

To confirm and to quantify the ¹⁸O enrichment in the FeO(OH) and Fe₂O₃ samples, the minerals were recovered and analyzed via secondary ion mass spectrometer (SIMS) (Methods section) (Figure 2 and Table S3). Prior to the

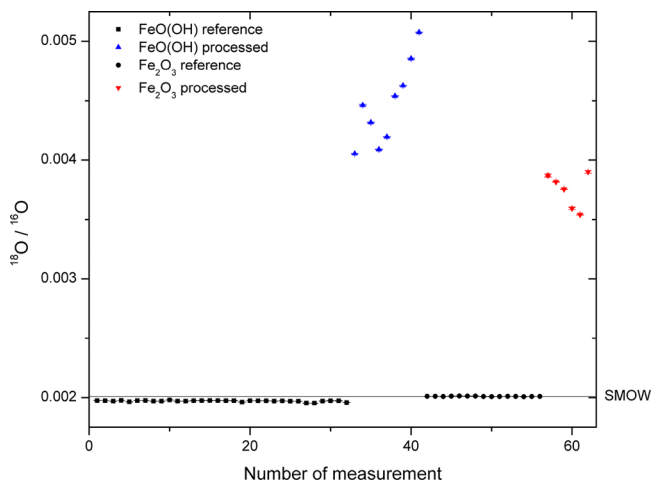
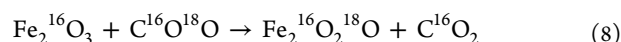
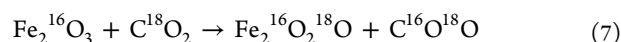
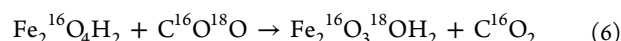
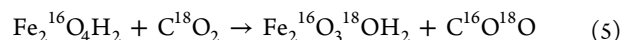


Figure 2. Ion microprobe results for the reference and processed samples. The black horizontal line labeled “SMOW” shows the Standard Mean Ocean Water value of ¹⁶O/¹⁸O = (2.005 ± 0.045) × 10⁻³. The error bars of the data points represent the calculated standard deviation of 30 cycles, each accumulated for 10 s.

exposure to carbon dioxide, the FeO(OH) and Fe₂O₃ samples exhibit ¹⁸O to ¹⁶O ratios of (1.971 ± 0.012) × 10⁻³ and (2.010 ± 0.004) × 10⁻³, respectively. These data are close to the VSMOW value of the ¹⁸O to ¹⁶O ratio of (2.005 ± 0.045) × 10⁻³.³⁰ After the processing, the FeO(OH) and Fe₂O₃ samples reveal ¹⁸O to ¹⁶O ratios of (4.5 ± 0.7) × 10⁻³ and (3.7 ± 0.3) × 10⁻³, i.e. an enrichment of ¹⁸O by a factor of 2.3 ± 0.4 and 1.9 ± 0.2 in FeO(OH) and Fe₂O₃, respectively. These quantitative findings show that both minerals lead to an ¹⁸O enrichment within the FeO(OH) and Fe₂O₃ minerals and simultaneously deplete ¹⁸O in gaseous carbon dioxide, with FeO(OH) resulting in a slightly enhanced ¹⁸O enrichment compared to Fe₂O₃.

First-principles electronic structure calculations using density functional theory (DFT) were performed to model the isotopic exchange reactions in question, with both accuracy and efficiency taken into consideration.³¹ Specifically, Gibbs free energy profiles were evaluated for the reactions between distinct carbon dioxide isotopologues (reaction 2, Figure 3a) and those between carbon dioxide isotopologues and models for goethite (reactions 5 and 6, Figure 3b) or hematite (reactions 7 and 8, Figure 3c):



Multiple bound structures of [FeO(OH)]₂-CO₂ and Fe₂O₃-CO₂ complexes were sampled as *simplified models* of possible reaction intermediates that involve carbon dioxide being chemisorbed on the surfaces of goethite and hematite. The noncatalytic reaction 2 exhibits an equilibrium constant

$$K_{\text{eq}} = [\text{C}^{16}\text{O}^{18}\text{O}]^2 / [\text{C}^{16}\text{O}_2][\text{C}^{18}\text{O}_2] = 3.9986 \quad (9)$$

and an adiabatic Gibbs free energy change $\Delta_r G = -3.3764 \text{ kJ mol}^{-1} \approx -3.4 \text{ kJ mol}^{-1}$ with the broken rotational symmetry of C¹⁶O¹⁸O as the main contributor. This adiabatic Gibbs free energy change corresponds to equilibrium fractions of 50%, 26%, and 24% for C¹⁶O¹⁸O, C¹⁶O₂, and C¹⁸O₂, which agree very well with the experimental observations reported in Figure 1a. As shown in Figure 3a, along the reaction path 2 for isotope exchange, two van der Waals complexes (or local minima, $\Delta G_{\text{vdw}} = +30.3 \text{ kJ mol}^{-1}$),³² two high-lying transition states ($\Delta G_{\text{ts}} = +270.4 \text{ kJ mol}^{-1}$), and one intermediate ($\Delta G_{\text{int}} = +223.2 \text{ kJ mol}^{-1}$) were identified, indicating a two-step isotopic exchange mechanism in the gas phase. However, the very high free energy barrier closes this channel at 293 K and indicates the necessity of a catalyst to reduce the effective barrier. This catalyst can be the wall of the container, or goethite, or hematite. Considering the chemical complexity of the Pyrex glass surface as discussed above, elucidating the surface-catalyzed reactions in the reference system by the Pyrex glass or by the glass-to-metal adapter of the gas storage device is beyond the scope of the present work.

Having established both experimentally and computationally that the isotopic exchange of carbon dioxide in the reference system can be replicated quantitatively in terms of thermodynamic equilibrium effects, we explored the roles of model [FeO(OH)]₂ and Fe₂O₃ clusters representing goethite and hematite, respectively, in the isotopic exchange mechanism(s). Based on experimental results, equilibrium constants of 4.28 and 4.15 can be obtained in the presence of goethite and hematite, respectively. This indicates unaltered overall thermodynamics although ¹⁸O is depleted at different levels.

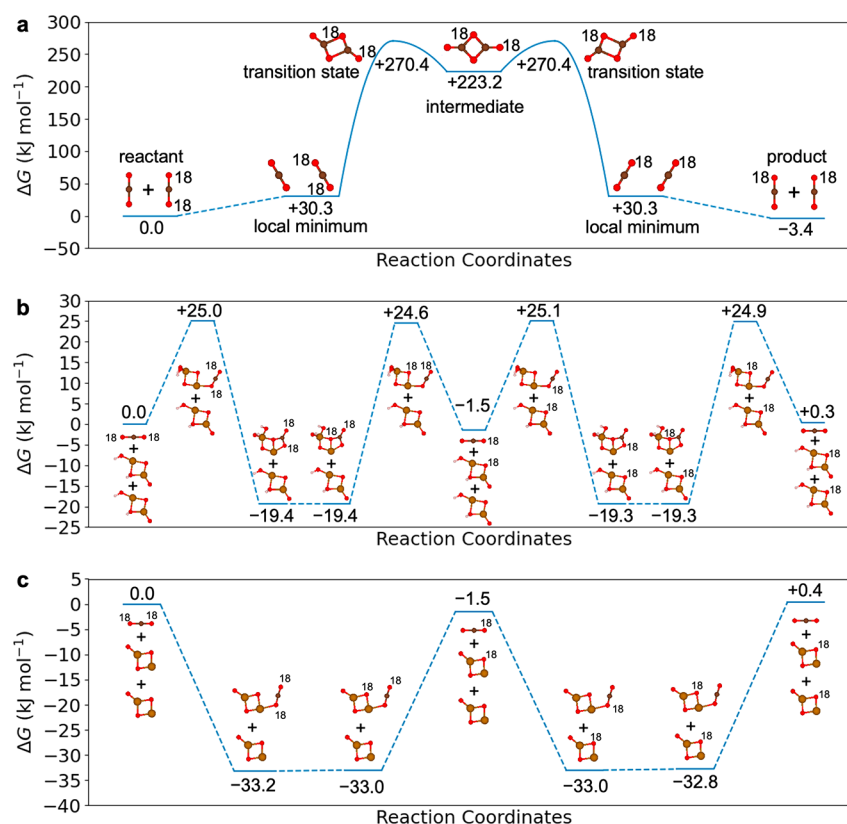
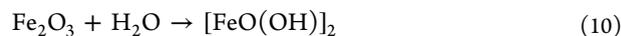


Figure 3. Calculated Gibbs free energies for representative isotopic exchange mechanisms: (a) reaction 2, (b) reactions 5–6, and (c) reactions 7–8. The total Gibbs free energies of the isolated reactants of reactions 2 ($C(^{18}O)_2$ and $C(^{16}O)_2$), 5 ($C(^{18}O)_2$ and $2Fe_2(OOH)_2$), and 7 ($C(^{18}O)_2$ and $2Fe_2O_3$) are set to zero for a, b, and c. Atoms that are included in the illustration are Fe (orange), C (brown), O (red, with ^{18}O labeled using 18), and H (white). Transition states are indicated by tops of parabolas. The Cartesian coordinates for the reactants, products, intermediates, and transition states are compiled in Tables S3–S8.

In our expanded computational consideration of detailed isotopic exchange mechanisms, the majority of bound $[FeO(OH)]_2-CO_2$ and $Fe_2O_3-CO_2$ intermediates sampled are nearly thermodynamically neutral ($|\Delta_r G| \leq 0.1 \text{ kJ mol}^{-1}$) for the exchange of ^{16}O and ^{18}O via elementary steps 5 through 8 and are thus not impactful. In a distinct portion of $[FeO(OH)]_2-CO_2$ configurations, interestingly, the symmetric and asymmetric stretching modes of the $C=O$ moiety in the CO_2 entity contribute to nontrivial Gibbs free energy changes and hence preferentially remove ^{18}O rather than ^{16}O from the gas-phase carbon dioxide. This reveals a qualitative agreement with experimental results illustrated in Figure 1b. As a typical example (Figure 3b), isotopic exchange can occur between CO_2 and a bridge O atom in $[FeO(OH)]_2$ through the $[FeO(OH)]_2-CO_2$ cluster, leading to $\Delta_r G = -0.4$ and -0.2 kJ mol^{-1} for reactions 5 and 6, respectively.

The oxygen isotopic cycle between oxygen-bearing molecules such as carbon dioxide in the Martian atmosphere and surface minerals like goethite and hematite has remained a highly controversial topic with atmospheric loss to space of the lighter ^{16}O , initially proposed as a driving force to account for the higher levels of ^{18}O in atmospheric carbon dioxide as determined by the Phoenix Lander and the Curiosity Rover of $\delta^{18}O = 31.0 \pm 5.7\%$ and $\delta^{18}O = 48 \pm 5\%$, respectively.^{18,33} However, hitherto unspecified heterogeneous processes involving minerals in the Martian soil were proposed to play a critical role in the oxygen isotopic enrichment in the Martian atmosphere.¹⁸ Our present study provides compelling evidence that hematite (iron(III) oxide, Fe_2O_3) and goethite (ferric

oxide hydroxide, $(FeO(OH))_2$)—two ubiquitous minerals on the surface of Mars with total average weight percentages of about 18% based on data from the Viking Lander and Pathfinder Missions—drive an oxygen isotopic exchange between atmospheric carbon dioxide and the minerals. This leads to an ^{18}O enrichment in the iron-containing minerals. This isotopic exchange operates in the dark, i.e., without illumination of the samples with light, and at temperatures at least as low as 293 K. Furthermore, our experiments provide the proof-of-concept that the ^{18}O – ^{16}O exchange between the atmosphere and the minerals is facile and slightly accelerated in goethite compared to hematite. Considering that hematite can be transformed into goethite upon exposure to water on Mars formally via eq 10



the oxygen isotopic enrichment on the Martian surface is expected to be accelerated in “wet” areas compared to dry regions. By contrast, dehydration of goethite to hematite requires temperatures above 500 K.³⁴ Although bulk liquid water has not been detected on the present Martian surface so far, numerous researchers have suggested that brines or interfacial water may occur periodically based on contemporary gully activity, dune and slope streaks, and recurring lineae.^{35–39} Because water sublimation and condensation on Mars remains an active, ongoing process, this might also challenge the generally accepted hypothesis that the present composition of the Martian atmosphere represents the end-

product of the planetary evolution over the age of our Solar System.

To conclude, our findings represent a step toward a better understanding of the critical role of distinct minerals on the Martian surface in ^{18}O isotopic exchange processes between atmospheric carbon dioxide and surface minerals. Although these investigations were conducted at 293 K, whereas the average surface temperature of Mars resides at 210 K,⁴⁰ these results also highlight the necessity to incorporate—besides the traditional gas-phase atmospheric chemistry—heterogeneous chemistry into future atmospheric and surface models in an attempt to replicate isotopic enrichments in the Martian atmosphere and on the surface. It is worth noting, however, that the surface on Mars may reach the temperatures at which our experiments were conducted (293 K) at noon in the summer in the equatorial area.^{7–11} It should be highlighted that no single laboratory setup can replicate the complexity of the physical and chemical parameters in “real” planetary environments. Future studies should unravel how the isotopic exchange depends, for instance, on lower temperatures and pressures. Likewise, potential synergistic effects of simultaneous exposure to light on the ^{18}O enrichment pathways should be untangled as well as how these processes depend on the wavelength of the light and on the grain size of the minerals. The interaction of carbon dioxide with goethite surfaces may also involve carbonate intermediates, which could be traced in future experiments.⁴¹ Finally, distinct minerals and mixtures have to be explored and how the chemical composition might lead to distinct isotopic fractionation. Finally, electronic structure computations played a critical role in supporting our experimental findings. Distinct structures of clusters such as in the goethite model system can qualitatively account for preferential depletion of ^{18}O from gas-phase carbon dioxide to the mineral as determined experimentally. However, because of the complexity of the solid-state system and potential effects of grain sizes, interstitial sites, and the solid-state structure versus model clusters, the computational observations cannot quantitatively simulate the experimental ones. Nevertheless, our combined experimental and computational study presents an explicit proof-of-concept of the ^{18}O depletion from gas-phase carbon dioxide to goethite, thus giving us a broader understanding of the processes responsible for isotope abundance ratios on Mars. The same ideas may also be relevant in the solar nebula where temperatures exceed 273 K within 3–4 astronomical units (AU) from the Sun.

EXPERIMENTAL AND COMPUTATIONAL METHODS

Equimolar mixtures of carbon dioxide (C^{16}O_2) and ^{18}O -carbon dioxide (C^{18}O_2) were prepared at a temperature of 293 ± 1 K in three separate Pyrex sample containers at a volume of 24 ± 1 mL by filling each vial with 60 ± 1 mbar of C^{16}O_2 (Airgas, 99.999%) and 60 ± 1 mbar of C^{18}O_2 (Sigma-Aldrich, 95 atom % ^{18}O), respectively. Two of the vials also contained goethite (ferric oxide hydroxide, $\text{FeO}(\text{OH})$, Sigma-Aldrich) and hematite (iron(III) oxide, Fe_2O_3 , Sigma-Aldrich); the third vial acted as a reference and hence did not contain any added iron oxide. To monitor the isotopic exchange, the individual gas mixtures were effused in well-defined time intervals into an ultrahigh-vacuum chamber at a pressure of $(9.0 \pm 0.1) \times 10^{-9}$ mbar, and the composition was analyzed via an electron impact residual gas analyzer (quadrupole mass spectrometer, EI-QMS) for the C^{16}O_2 , $\text{C}^{16}\text{O}^{18}\text{O}$, and C^{18}O_2

isotopologues of carbon dioxide.⁴² Finally, the goethite and hematite samples were recovered from the vials, and the ^{18}O enrichment was determined exploiting a Cameca IMS-1280 secondary ion mass spectrometer (SIMS). We would like to stress that the vessel and the samples were baked while simultaneously pumping the system to ultrahigh-vacuum conditions (10^{-10} Torr) to remove any potential water contaminations. This protocol has been well-established to eliminate even traces of water.⁴³ Furthermore, the absence of any water was confirmed spectroscopically. We recorded in separate experiments infrared spectra (FTIR) of the gases effused into the vacuum system; not even traces of water impurities were observed (Figure S1 and Table S2).

The Pfeiffer Vacuum QMG 422 was operated with an electron impact ionization energy of 100 eV and an emission current of 0.7 mA; ions were detected by a secondary electron multiplier held at 2000 V. At these conditions, ion–molecule reactions were found not to induce any isotopic scrambling in the C^{16}O_2 – C^{18}O_2 gas mixture.⁴⁴ After the experiments, the oxygen-isotope compositions were determined with a Cameca IMS-1280 secondary ion mass spectrometer (SIMS).⁴⁵ All samples were coated with gold (Au). A 1.5 nA focused cesium primary ion beam (Cs^+), accelerated to 10 keV, was rastered over a $25 \times 25 \mu\text{m}^2$ area of each sample for 120 s to remove the gold coating. The raster was then reduced to $15 \times 15 \mu\text{m}^2$ for data collection. The SIMS was operated at a potential of -10 keV, meaning 20 keV impact energy for the primary ions; a normal-incidence electron flood gun was used for charge compensation. The two oxygen isotopes were collected by using multicollection mode; $^{16}\text{O}^-$ and $^{18}\text{O}^-$ were measured on multicollector Faraday cups (FCs) with 10^{10} and $10^{11} \Omega$ resistors, respectively. Typical count rates of ^{16}O from $\text{FeO}(\text{OH})$ and Fe_2O_3 were $2 \times 10^9 \text{ s}^{-1}$. The mass-resolving power for $^{16}\text{O}^-$ and $^{18}\text{O}^-$ was set to 2000, which was sufficient to discriminate interfering ions. Each measurement consisted of 30 cycles with 10 s integration time per cycle. The reported ^{18}O to ^{16}O ratios were corrected for the relative detection efficiencies of the FCs and backgrounds. The $^{18}\text{O}/^{16}\text{O}$ isotopic ratios of $\text{FeO}(\text{OH})$ and Fe_2O_3 prior to exposure to the carbon dioxide gas mixture were also determined within the same experimental setup and act as reference data of the unprocessed material.

All electronic structure calculations were performed by using density functional theory (DFT) in Q-Chem 5.1⁴⁶ with the $\omega\text{B97M-V}$ exchange–correlation functional⁴⁷ and the def2-TZVPPD basis set.⁴⁸ Thermodynamic corrections were evaluated from vibrational–torsional and rotational degrees of freedom based on the quasi-rigid-rotor–harmonic oscillator (QRRHO)⁴⁹ model and experimental conditions ($T = 293$ K, partial pressure $p = 60$ mbar). This pressure does not agree with the partial pressures of carbon dioxide isotopologues in the Martian atmosphere, but it only impacts on the translational Gibbs free energy which is canceled between reactants and products. Transition states were obtained for reaction 2 by locating the first-order stationary point on the electronic potential energy surface (PES), which was confirmed by using the intrinsic reaction coordinate (IRC) approach.⁵⁰ In detailed mechanistic studies, CO_2 monomer and dimers, one Fe_2O_3 cluster, seven $[\text{FeO}(\text{OH})]_2$ clusters, four Fe_2O_3 – CO_2 clusters, and 24 $[\text{FeO}(\text{OH})]_2$ – CO_2 clusters were investigated at their optimized geometries that are presented as Cartesian coordinates in the Supporting Information.

■ ASSOCIATED CONTENT

SI Supporting Information

The Supporting Information is available free of charge at <https://pubs.acs.org/doi/10.1021/acs.jpcllett.2c00289>.

Summary of previous experimental studies of heterogeneous isotope exchange with metal oxides; FTIR spectra of the $C^{16}O_2-C^{18}O_2$ system at 10 K with full assignment; ion microprobe results of the reference and processed samples; computational details of the Gibbs free energy changes associated with isotopic exchange reactions using DFT; summaries of DFT-evaluated coordinates, harmonic frequencies, vibrational–torsional, and rotational Helmholtz free energies for species relevant to isotopic exchange reactions; DFT-evaluated and previously reported temperature dependence of equilibrium constant of the gas-phase isotopic exchange reaction (PDF)

■ AUTHOR INFORMATION

Corresponding Authors

Ralf I. Kaiser – Department of Chemistry, University of Hawai'i at Mānoa, Honolulu, Hawaii 96822, United States; W.M. Keck Laboratory in Astrochemistry, University of Hawai'i at Mānoa, Honolulu, Hawaii 96822, United States; orcid.org/0000-0002-7233-7206; Email: ralfk@hawaii.edu

Martin Head-Gordon – Kenneth S. Pitzer Center for Theoretical Chemistry, Department of Chemistry, University of California, Berkeley, Berkeley, California 94720, United States; orcid.org/0000-0002-4309-6669; Email: mhg@cchem.berkeley.edu

Authors

Sándor Góbi – Department of Chemistry, University of Hawai'i at Mānoa, Honolulu, Hawaii 96822, United States; W.M. Keck Laboratory in Astrochemistry, University of Hawai'i at Mānoa, Honolulu, Hawaii 96822, United States; orcid.org/0000-0002-7039-8099

Zhou Lin – Kenneth S. Pitzer Center for Theoretical Chemistry, Department of Chemistry, University of California, Berkeley, Berkeley, California 94720, United States; Department of Chemistry, University of Massachusetts, Amherst, Massachusetts 01003, United States; orcid.org/0000-0003-3271-5345

Cheng Zhu – Department of Chemistry, University of Hawai'i at Mānoa, Honolulu, Hawaii 96822, United States; W.M. Keck Laboratory in Astrochemistry, University of Hawai'i at Mānoa, Honolulu, Hawaii 96822, United States

Complete contact information is available at: <https://pubs.acs.org/doi/10.1021/acs.jpcllett.2c00289>

Author Contributions

S.G. and Z.L. contributed equally to this work.

Notes

The authors declare no competing financial interest.

■ ACKNOWLEDGMENTS

This work was supported by the National Aeronautics and Space Administration under Grant NNX14AG39G. We are grateful to Gary Huss and Kazuhide Nagashima at the W. M. Keck Cosmochemistry Laboratory of the University of Hawai'i at Mānoa for performing the SIMS measurements. Z.L. was

supported by the U.S. Department of Energy Office of Science, Basic Energy Sciences, under Contract DE-AC02-05CH11231. M.H.G. acknowledges support from the U.S. Department of Energy Office of Science, Advanced Scientific Computing Research and Basic Energy Sciences, via the Scientific Discovery through Advanced Computing (SciDAC) program.

■ REFERENCES

- (1) Thiemens, M. H.; Jackson, T. L.; Brenninkmeijer, C. A. M. Observation of a mass independent oxygen isotopic composition in terrestrial stratospheric CO_2 , the link to ozone chemistry, and the possible occurrence in the Martian atmosphere. *Geophys. Res. Lett.* **1995**, *22* (3), 255–257.
- (2) Alday, J.; Wilson, C. F.; Irwin, P. G. J.; Trokhimovskiy, A.; Montmessin, F.; Fedorova, A. A.; Belyaev, D. A.; Olsen, K. S.; Korabev, O.; Lefèvre, F.; et al. Isotopic composition of CO_2 in the atmosphere of Mars: Fractionation by diffusive separation observed by the ExoMars trace gas orbiter. *J. Geophys. Res.: Planets* **2021**, *126* (12), No. e2021JE006992.
- (3) Farquhar, J.; Thiemens, M. H.; Jackson, T. Atmosphere-surface interactions on Mars: $\Delta^{17}O$ measurements of carbonate from ALH 84001. *Science* **1998**, *280* (5369), 1580–1582.
- (4) Ali, A.; Jabeen, I.; Gregory, D.; Verish, R.; Banerjee, N. R. New triple oxygen isotope data of bulk and separated fractions from SNC meteorites: Evidence for mantle homogeneity of Mars. *Meteorit. Planet. Sci.* **2016**, *51* (5), 981–995.
- (5) Bellucci, J. J.; Whitehouse, M. J.; Nemchin, A. A.; Snape, J. F.; Kenny, G. G.; Merle, R. E.; Bland, P. A.; Benedix, G. K. Tracing Martian surface interactions with the triple O isotope compositions of meteoritic phosphates. *Earth Planet. Sci. Lett.* **2020**, *531*, 115977.
- (6) Peri, J. B. Oxygen exchange between $C^{18}O_2$ and “acidic” oxide and zeolite catalysts. *J. Phys. Chem.* **1975**, *79* (15), 1582–1588.
- (7) Hess, S. L.; Henry, R. M.; Leovy, C. B.; Ryan, J. A.; Tillman, J. E. Meteorological results from the surface of Mars: Viking 1 and 2. *J. Geophys. Res.* **1977**, *82* (28), 4559–4574.
- (8) Christensen, P. R.; Bandfield, J. L.; Hamilton, V. E.; Ruff, S. W.; Kieffer, H. H.; Titus, T. N.; Malin, M. C.; Morris, R. V.; Lane, M. D.; Clark, R. L.; et al. Mars Global Surveyor Thermal Emission Spectrometer experiment: Investigation description and surface science results. *J. Geophys. Res.: Planets* **2001**, *106* (E10), 23823–23871.
- (9) Spanovich, N.; Smith, M. D.; Smith, P. H.; Wolff, M. J.; Christensen, P. R.; Squyres, S. W. Surface and near-surface atmospheric temperatures for the Mars Exploration Rover landing sites. *Icarus* **2006**, *180* (2), 314–320.
- (10) Stillman, D. E.; Michaels, T. I.; Grimm, R. E.; Harrison, K. P. New observations of Martian southern mid-latitude recurring slope lineae (RSL) imply formation by freshwater subsurface flows. *Icarus* **2014**, *233*, 328–341.
- (11) McCleese, D. J.; Heavens, N. G.; Schofield, J. T.; Abdou, W. A.; Bandfield, J. L.; Calcutt, S. B.; Irwin, P. G. J.; Kass, D. M.; Kleinböhl, A.; Lewis, S. R.; et al. Structure and dynamics of the Martian lower and middle atmosphere as observed by the Mars Climate Sounder: Seasonal variations in zonal mean temperature, dust, and water ice aerosols. *J. Geophys. Res.: Planets* **2010**, *115*, No. E12016.
- (12) Stolper, E.; Epstein, S. An experimental study of oxygen isotope partitioning between silica glass and CO_2 vapor. In *Stable Isotope Geochemistry: A Tribute to Samuel Epstein*; Special Publication (Geochemical Society) No. 3; Geochemical Society: San Antonio, TX, 1991; pp 35–51.
- (13) Nie, N. X.; Dauphas, N.; Greenwood, R. C. Iron and oxygen isotope fractionation during iron UV photo-oxidation: Implications for early Earth and Mars. *Earth Planet. Sci. Lett.* **2017**, *458*, 179–191.
- (14) Kurokawa, H.; Sato, M.; Ushioda, M.; Matsuyama, T.; Moriwaki, R.; Dohm, J. M.; Usui, T. Evolution of water reservoirs on Mars: Constraints from hydrogen isotopes in Martian meteorites. *Earth Planet. Sci. Lett.* **2014**, *394*, 179–185.

- (15) Wright, I. P.; Grady, M. M.; Pillinger, C. T. Carbon, oxygen and nitrogen isotopic compositions of possible Martian weathering products in EETA 79001. *Geochim. Cosmochim. Acta* **1988**, *52* (4), 917–924.
- (16) Niles, P. B.; Catling, D. C.; Berger, G.; Chassefière, E.; Ehlmann, B. L.; Michalski, J. R.; Morris, R.; Ruff, S. W.; Sutter, B. Geochemistry of carbonates on Mars: Implications for climate history and nature of aqueous environments. *Space Sci. Rev.* **2013**, *174* (1–4), 301–328.
- (17) Halevy, I.; Fischer, W. W.; Eiler, J. M. Carbonates in the Martian meteorite Allan Hills 84001 formed at 18 ± 4 °C in a near-surface aqueous environment. *Proc. Natl. Acad. Sci. U. S. A.* **2011**, *108* (41), 16895–16899.
- (18) Webster, C. R.; Mahaffy, P. R.; Flesch, G. J.; Niles, P. B.; Jones, J. H.; Leshin, L. A.; Atreya, S. K.; Stern, J. C.; Christensen, L. E.; Owen, T.; Franz, H.; Pepin, R. O.; Steele, A. Isotope ratios of H, C, and O in CO₂ and H₂O of the Martian atmosphere. *Science* **2013**, *341* (6143), 260–263.
- (19) Shaheen, R.; Niles, P. B.; Chong, K.; Corrigan, C. M.; Thiemens, M. H. Carbonate formation events in ALH 84001 trace the evolution of the Martian atmosphere. *Proc. Natl. Acad. Sci. U. S. A.* **2015**, *112* (2), 336–341.
- (20) Shaheen, R.; Abramian, A.; Horn, J.; Dominguez, G.; Sullivan, R.; Thiemens, M. H. Detection of oxygen isotopic anomaly in terrestrial atmospheric carbonates and its implications to Mars. *Proc. Natl. Acad. Sci. U. S. A.* **2010**, *107* (47), 20213–20218.
- (21) Leshin, L. A.; McKeegan, K. D.; Carpenter, P. K.; Harvey, R. P. Oxygen isotopic constraints on the genesis of carbonates from Martian meteorite ALH84001. *Geochim. Cosmochim. Acta* **1998**, *62* (1), 3–13.
- (22) Mills, G. A.; Urey, H. C. The kinetics of isotopic exchange between carbon dioxide, bicarbonate ion, carbonate ion and water. *J. Am. Chem. Soc.* **1940**, *62* (5), 1019–1026.
- (23) Clayton, R. N.; Mayeda, T. K. Isotopic composition of carbonate in EETA 79001 and its relation to parent body volatiles. *Geochim. Cosmochim. Acta* **1988**, *52* (4), 925–927.
- (24) Krasnopolsky, V. A.; Mumma, M. J.; Bjoraker, G. L.; Jennings, D. E. Oxygen and carbon isotope ratios in Martian carbon dioxide: Measurements and implications for atmospheric evolution. *Icarus* **1996**, *124* (2), 553–568.
- (25) Morris, R. V.; Klingelhofer, G.; Schröder, C.; Rodionov, D. S.; Yen, A.; Ming, D. W.; de Souza, P. A., Jr.; Fleischer, I.; Wdowiak, T.; Gellert, R.; et al. Mössbauer mineralogy of rock, soil, and dust at Gusev crater, Mars: Spirit's journey through weakly altered olivine basalt on the plains and pervasively altered basalt in the Columbia Hills. *J. Geophys. Res. Planets* **2006**, *111*, No. E02S13.
- (26) Allen, C. C.; Jager, K. M.; Morris, R. V.; Lindstrom, D. J.; Lindstrom, M. M.; Lockwood, J. P. JSC Mars-1: A Martian soil simulant. In *Proceedings of Space 98: Sixth International Conference and Exposition on Engineering, Construction, and Operations in Space, Albuquerque, NM, 1998*; pp 469–476.
- (27) Li, S.; Lucey, P. G.; Fraeman, A. A.; Poppe, A. R.; Sun, V. Z.; Hurley, D. M.; Schultz, P. H. Widespread hematite at high latitudes of the Moon. *Sci. Adv.* **2020**, *6* (36), No. eaba1940.
- (28) Shkrob, I. A.; Chemerisov, S. D.; Marin, T. W. Photocatalytic decomposition of carboxylated molecules on light-exposed Martian regolith and its relation to methane production on Mars. *Astrobiology* **2010**, *10* (4), 425–436.
- (29) Steinfeld, J. I.; Francisco, S. F.; Hase, W. L. *Chemical Kinetics and Dynamics*, 2nd ed.; Prentice Hall: Upper Saddle River, NJ, 1999.
- (30) Criss, R. E. *Principles of Stable Isotope Distribution*; Oxford University Press: Oxford, UK, 1999.
- (31) Mardirossian, N.; Head-Gordon, M. Thirty years of density functional theory in computational chemistry: An overview and extensive assessment of 200 density functionals. *Mol. Phys.* **2017**, *115* (19), 2315–2372.
- (32) Dehghany, M.; McKellar, A. R. W.; Afshari, M.; Moazzen-Ahmadi, N. High-resolution infrared spectroscopy of carbon dioxide dimers, trimers, and larger clusters. *Mol. Phys.* **2010**, *108* (17), 2195–2205.
- (33) Niles, P. B.; Boynton, W. V.; Hoffman, J. H.; Ming, D. W.; Hamara, D. Stable isotope measurements of Martian atmospheric CO₂ at the Phoenix landing site. *Science* **2010**, *329* (5997), 1334–1337.
- (34) Özdemir, Ö.; Dunlop, D. J. Intermediate magnetite formation during dehydration of goethite. *Earth Planet. Sci. Lett.* **2000**, *177* (1–2), 59–67.
- (35) Malin, M. C.; Edgett, K. S.; Posiolova, L. V.; McColley, S. M.; Dobrea, E. Z. N. Present-day impact cratering rate and contemporary gully activity on Mars. *Science* **2006**, *314* (5805), 1573–1577.
- (36) Kreslavsky, M. A.; Head, J. W. Slope streaks on Mars: A new “wet” mechanism. *Icarus* **2009**, *201* (2), 517–527.
- (37) McEwen, A. S.; Ojha, L.; Dundas, C. M.; Mattson, S. S.; Byrne, S.; Wray, J. J.; Cull, S. C.; Murchie, S. L.; Thomas, N.; Gulick, V. C. Seasonal flows on warm Martian slopes. *Science* **2011**, *333* (6043), 740–743.
- (38) Kereszturi, A.; Gobi, S. Possibility of H₂O₂ decomposition in thin liquid films on Mars. *Planet. Space Sci.* **2014**, *103*, 153–166.
- (39) Martín-Torres, F. J.; Zorzano, M.-P.; Valentin-Serrano, P.; Harri, A.-M.; Genzer, M.; Kemppinen, O.; Rivera-Valentin, E. G.; Jun, I.; Wray, J.; Bo Madsen, M.; et al. Transient liquid water and water activity at Gale crater on Mars. *Nat. Geosci.* **2015**, *8* (5), 357–361.
- (40) Kieffer, H. H.; Jakosky, B. M.; Snyder, C. W.; Matthews, M. S. *Mars*; University of Arizona Press: Tucson, AZ, 1992.
- (41) Russell, J. D.; Paterson, E.; Fraser, A. R.; Farmer, V. C. Adsorption of carbon dioxide on goethite (α -FeOOH) surfaces, and its implications for anion adsorption. *J. Chem. Soc., Faraday Trans. 1* **1975**, *71*, 1623–1630.
- (42) Bennett, C. J.; Jamieson, C.; Mebel, A. M.; Kaiser, R. I. Untangling the formation of the cyclic carbon trioxide isomer in low temperature carbon dioxide ices. *Phys. Chem. Chem. Phys.* **2004**, *6* (4), 735–746.
- (43) Zhu, C.; Góbi, S.; Abplanalp, M. J.; Frigge, R.; Gillis-Davis, J. J.; Dominguez, G.; Miljković, K.; Kaiser, R. I. Regenerative water sources on surfaces of airless bodies. *Nat. Astron.* **2020**, *4* (1), 45–52.
- (44) Bennett, C. J.; Jamieson, C. S.; Kaiser, R. I. Mechanical studies on the formation and destruction of carbon monoxide (CO), carbon dioxide (CO₂), and carbon trioxide (CO₃) in interstellar ice analog samples. *Phys. Chem. Chem. Phys.* **2010**, *12* (16), 4032–4050.
- (45) Nagashima, K.; Huss, G. R.; Kosaka, K.; Kunihiro, T.; Keil, K.; Krot, A. N.; Taylor, G. J.; Yurimoto, H. Development of isotope imaging system with two-dimensional ion detector SCAPS for IMS-1280 secondary ion mass spectrometer. In *40th Annual Lunar and Planetary Science Conference, Woodland, TX, 2009*; p 2066.
- (46) Shao, Y.; Gan, Z.; Epifanovsky, E.; Gilbert, A. T.; Wormit, M.; Kussmann, J.; Lange, A. W.; Behn, A.; Deng, J.; Feng, X.; et al. Advances in molecular quantum chemistry contained in the Q-Chem 4 program package. *Mol. Phys.* **2015**, *113* (2), 184–215.
- (47) Mardirossian, N.; Head-Gordon, M. ω B97M-V: A combinatorially optimized, range-separated hybrid, meta-GGA density functional with TV10 nonlocal correlation. *J. Chem. Phys.* **2016**, *144* (21), 214110.
- (48) Rappoport, D.; Furche, F. Property-optimized Gaussian basis sets for molecular response calculations. *J. Chem. Phys.* **2010**, *133* (13), 134105.
- (49) Grimme, S. Supramolecular binding thermodynamics by dispersion-corrected density functional theory. *Chem.—Eur. J.* **2012**, *18* (32), 9955–9964.
- (50) Fukui, K. Formulation of the reaction coordinate. *J. Phys. Chem.* **1970**, *74* (23), 4161–4163.